3D Patterning at the Nanoscale of Fluorescent Emitters in Glass

Matthieu Bellec,[†] Arnaud Royon,[†] Kevin Bourhis,[‡] Jiyeon Choi,[‡,§] Bruno Bousquet,[†] Mona Treguer,[‡] Thierry Cardinal,[‡] Jean-Jacques Videau,[‡] Martin Richardson,[§] and Lionel Canioni*,[†]

Centre de Physique Moléculaire Optique et Hertzienne, UMR 5798 CNRS, Université de Bordeaux, 351 cours de la Libération, 33405 Talence Cedex, France, Institut de Chimie de la Matière Condensée de Bordeaux—UPR 9048 CNRS, Université de Bordeaux, Avenue du Dr. Schweitzer, 33608 Pessac Cedex, France, and College of Optics and Photonics/CREOL, University of Central Florida, 4000 Central Florida Boulevard, Orlando, Florida 32816

Received: May 4, 2010; Revised Manuscript Received: July 26, 2010

Three-dimensional fluorescent nanostructures are photoinduced by a near-infrared high repetition rate femtosecond laser in a silver-containing femto-photoluminescent glass. By adjusting the laser dose (fluence, number of pulses, and repetition rate), these stabilized intense fluorescent structures, composed of silver clusters, can be achieved with a perfect control of the luminescence intensity, the emission spectrum, and the spatial distribution at the nanometer scale. This novel approach opens the way to the fabrication of stable fluorescent nanostructures in three dimensions in glass for applications in photonics and optical data storage.

1. Introduction

Silver clusters stabilized in different matrixes have been reported to exhibit intense fluorescence properties.[1−4] Multiple applications have been proposed from biological labeling for clusters in water,[5] in polymer,[6] and radiation dosimetry when generated in a glass matrix.[7−9] The generation and stabilization of these species is one of the main issues. For the fabrication, two approaches have been used, starting from the metal bulk or the silver ions. In the case of the metallic thin film, silver photodissociation and oxidation give rise to the formation of silver oligomers.[10] In the case of silver ions in a solid state matrix under ionizing radiation, photographic-like processes have been carried out in order to generate electron trap and hole centers that have been identified as Ag^0 and Ag^{2+} species leading later, through a migration process by chemical treatment, to the formation of Ag_n nanoparticles.[11]

Moreover, in the last fifteen years, direct laser writing techniques have allowed three-dimensional (3D) microstructuring mainly through the modification of the refractive index in transparent materials and have been widely used for photonics applications,[12] such as waveguides[13,14] and optical data storage.[15,16] Concerning the size, it has been proven that nonlinear localized polymerization allows structuring well below the diffraction limit.[17] With additional tooling costs, lithographic techniques (usually limited to 2D) can be extended also to 3D using layer-on-layer approaches to obtain nanoscale structures.[18] Recently, a technique that combines direct laser writing and metal deposition permits the creation of nanostructures.[19] However, all these techniques suffer from several drawbacks that include slow processing speeds, complexity in implementation, and the availability of materials and patterns.

In this paper, we use a near-infrared (NIR) high repetition rate femtosecond laser to fabricate 3D fluorescent nanostructures with a size well below the diffraction limit in a silver-containing glass, named, hereafter, femto-photoluminescent (FPL) glass. We demonstrate that stabilized intense fluorescent structures, composed of silver clusters, can be achieved with a perfect control of the luminescence properties and the spatial distribution at the nanometer scale.

2. Experimental Methods

2.1. Glass Fabrication. Glasses with the composition $40P_2O_5-4Ag_2O-55ZnO-1Ga_2O_3$ (mol %) were made using a standard melt quench technique. $(NH_4)_2HPO_4$, ZnO, $AgNO_3$, and Ga_2O_3 in powder form were used as raw materials, and the proper amount was placed in a platinum crucible. A heating rate of about 1 °C·min^{-1} was used up to 1000 °C. The melt was then kept at this last temperature (1000 °C) from 24 to 48 h. Following this step, the liquid was poured into a brass mold after a short increase of the temperature at 1100 °C in order to access the appropriate viscosity. The glass samples obtained were annealed at 320 °C (55 °C below the glass transition temperature) for 3 h, cut (0.5−1 mm thick), and optically polished.

2.2. 3D Direct Laser Structuring. The glass sample was irradiated using a femtosecond laser oscillator source emitting 470 fs, 10 MHz repetition rate pulses at 1030 nm. The laser mode is TEM_{00}, $M^2 = 1.2$, and the output polarization is TM. The maximum output average power is close to 5 W, which results in a maximum energy per pulse of 500 nJ. Acousto-optic filtering permits the tuning of the pulse energy, the number of pulses, and the repetition rate for control of the cumulated effects. The femtosecond laser is focused using a reflective 36× objective with a 0.52 NA (working distance = 15 mm) at a depth of 200 μm in the glass. The beam waist is estimated to be 1 μm. The sample was manipulated using a microprecision *xyz* stage.

2.3. Fluorescence Microscopy. The fluorescence images and spectra were performed with a confocal microscope (Leica TCS SP2). The fluorescence lifetime was measured by a fluorescence

* To whom correspondence should be addressed. E-mail: l.canioni@cpmoh.u-bordeaux1.fr. Phone: +33 (0)5 40 00 83 25.
[†] Centre de Physique Moléculaire Optique et Hertzienne, UMR 5798 CNRS, Université de Bordeaux.
[‡] Institut de Chimie de la Matière Condensée de Bordeaux—UPR 9048 CNRS, Université de Bordeaux.
[§] University of Central Florida.

10.1021/jp104049e

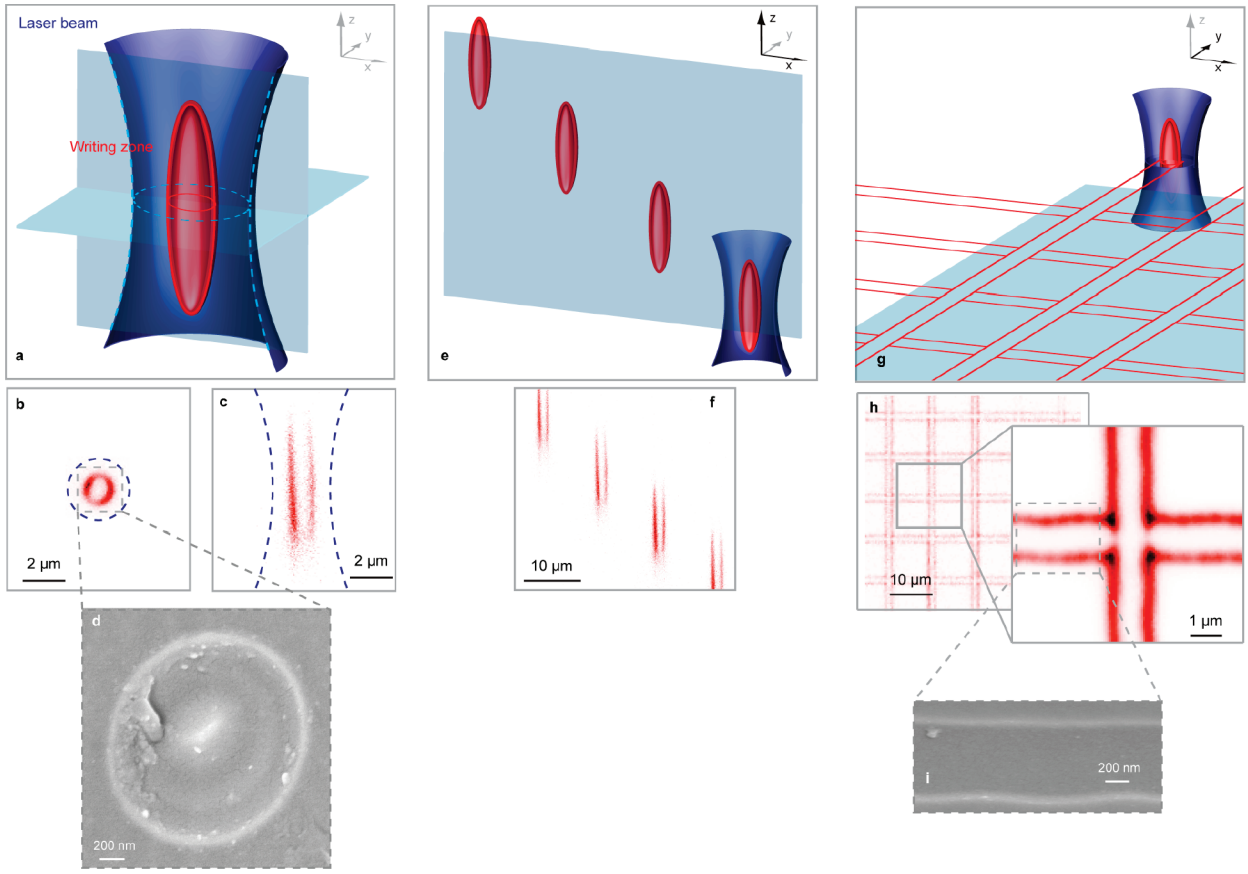

Figure 1. Configurations of the laser writing process inside the glass with a stationary focus (a), at different depths (e), and in the same plane (g). Fluorescence images (λ_{exc} = 405 nm) of the nanostructures in the *xy* (b) and *xz* (c) planes. Fluorescence images of patterns written at different depths (f) and in the same plane (h). The insets (d) and (i) correspond to HRSEM images of (b) and (h) indicating that the fluorescent clusters are organized at the nanoscale.

lifetime imaging microscope (FLIM) composed of a titanium: sapphire laser tunable from 730 to 980 nm delivering 200 fs pulses at 76 MHz (Mira Coherent) and a confocal microscope (Leica TCS SP2) equipped with an FLIM acquisition system (Becker-Hickl).

2.4. High Reflection Scanning Electron Microscopy. A high reflection scanning electron microscope (HRSEM JEOL 6700F, gun field emission, resolution = 1.1 nm) was used for irradiated sample analysis. It is of great interest to note that HRSEM allows both a topological (using secondary electron mode) and a chemical (using backscattered electron mode) characterization. Both configurations are used to image the nanostructures. Following femtosecond laser irradiation, the nanostructures present no topological changes. Thus, an acid treatment, 10 s in nitric acid, was performed on each sample to reveal the nanostructures. Acid etches preferentially the silver-containing area.

3. Results and Discussion

3.1. Glass Properties. The FPL glass has the following composition: $4Ag_2O-40P_2O_5-55ZnO-1Ga_2O_3$ (mol %). $ZnO-P_2O_5$ is the network former, Ag_2O is the photosensitive agent, and Ga_2O_3 is introduced to improve the chemical stability of the zinc phosphate glass matrix. The local chemical structure of this glass is close to a pyrophosphate and happens to be appropriate to stabilize photoinduced silver clusters. The FPL glass is transparent in the visible region. It exhibits an absorption cutoff at around 280 nm mainly due to the silver ions associated absorption. Fluorescence spectroscopy has shown an intrinsic main feature composed of an excitation band at 265 nm and a corresponding emission at 380 nm associated with the dipolar electric transition $4d^{10} \leftrightarrow 4d^9\,5s^1$ of the isolated Ag^+ silver ions. A weak emission observed at 520 nm, corresponding to the presence of Ag^+-Ag^+ pairs in small amounts, has already been mentioned by Belharouak et al. in similar glass compositions.[20]

3.2. Ring-Shaped Nanostructure Fabrication. The FPL glass has been irradiated by NIR femtosecond pulses focused with a microscope objective below the surface with different writing parameters (repetition rate, number of pulses, and irradiance, gathered into the dose). Four-photon absorption was shown to be the main mechanism for the laser−glass interaction.[21] Because of this nonlinear behavior, the photoinduced structures are created inside the focusing voxel, allowing 3D shaping (Figure 1a). After femtosecond laser irradiation, the sample presents a weak absorption between 280 and 410 nm corresponding to photoinduced clusters (see the Supporting Information). Excitation within this wavelength range leads to a broad visible emission. The photoinduced structures are composed of silver clusters arranged into a pipe shape along the propagation axis, with a length corresponding to the Rayleigh range (Figure 1c) and a wall thickness of 80 nm (Figure 1b,d). The section of this pipe is shown in Figure 1b, with a radius that depends on the irradiation conditions. The thickness of the ring in the fluorescence images is measured at about 300 nm, which corresponds to the spatial resolution of the confocal fluorescence microscope. The structure has been imaged by high-resolution scanning electron microscopy (HRSEM) (Figure 1d) after selective acid etching. In the backscattering mode, a

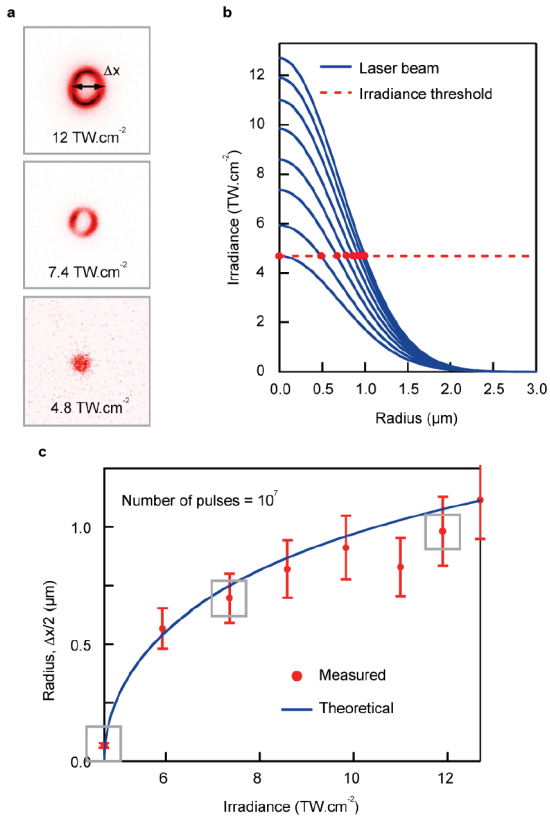

Figure 2. Feature size control. (a) Fluorescence images (λ_{exc} = 405 nm) of the photoinduced structures at three different irradiances (4.8, 7.4, and 12 TW·cm^{-2}) and 10^7 pulses. Above 4.8 TW·cm^{-2}, ring structures are observed. (b) Evolution of the laser irradiance versus the radius of the ring structures. This graph clearly shows that their formation is due to a threshold effect. (c) Evolution of the measured and calculated beam radius (fwhm) versus the laser irradiance. The computation is based on a diffusion model that takes into account the threshold effect. The three fluorescence images of (a) correspond to the framed dots of (c).

chemical contrast has been observed on the ring. Its thickness has been evaluated at roughly 80 nm and corresponds to the location of the maximum of fluorescence (more details are available in the Supporting Information).

3.3. Silver Cluster Formation Mechanism. The formation of the photoinduced silver clusters and their surprising arrangement into a ring shape perpendicular to the light propagation axis has been described earlier and can be summarized as follows.[21] A reservoir of "free" electrons is generated from multiphoton absorption, enabling the reduction of Ag^+ silver ions to the Ag^0 atomic state, which aggregates with silver ions, leading to the formation of Ag_2^+. Following a chain reaction, larger Ag_m^{x+} clusters are formed from Ag^+, Ag^0, and Ag_2^+ inside the glass matrix. The transverse Gaussian profile of the laser beam induces the photodissociation of the clusters in the central part of the beam.[21] The control of the irradiance allows for changing the radius of the ring structures, as shown by the fluorescence microscopy images in Figure 2a. Their formation is clearly related to a threshold effect (Figure 2b). Indeed, for a given number of pulses (10^7 pulses), no ring can be created below an irradiance of 4.8 TW·cm^{-2} (Figure 2c), but the photoinduced fluorescent structure follows the irradiance spatial profile of the laser beam. Above this irradiance, a ring is formed and its radius increases with the irradiance until it reaches a limit value of 1 μm, the size of the beam waist.

3.4. Nanostructure Fluorescence Properties. The photoinduced silver clusters exhibit remarkable fluorescence properties that are governed by the dose. These silver clusters are formed with irradiances below the refractive index modification threshold of the glass (12.5 TW·cm^{-2}, corresponding to a fluence of 6 J·cm^{-2}) so that these structures can be viewed only through their fluorescence. Thanks to the nonlinear interaction, fluorescent patterns can be drawn in 3D. For such a purpose, the sample is moved in the three directions relative to the laser beam waist. Figure 1e,f represents patterns written at different depths, and Figure 1g−i represents patterns written in the same plane. With 3D control of the motion, complete fluorescent nanostructures can be achieved.

The fluorescence properties (intensity, spectrum, and lifetime) of the silver clusters depend in different ways on the repetition rate, the irradiance, and the number of pulses deposited (Figure 3a−c). First, the fluorescence intensity for excitation at 405 nm is strongly correlated to the repetition rate of the laser. Indeed, by decreasing the repetition rate of the laser by a factor of 10, the irradiance and the number of pulses being kept the same, the fluorescence intensity decreases by a factor of 5 (Figure 3b). By decreasing it again by a factor of 10, the fluorescence almost disappears (Figure 3c). At a low repetition rate (100 kHz), the characteristic thermal relaxation time becomes short compared with the laser period so that the thermal effects are not cumulative. On the contrary, at a high repetition rate (10 MHz), cumulative effects occur and the temperature increases pulse after pulse, approaching the glass transition temperature.[21] This thermodiffusion process allows silver atoms and ions to diffuse and aggregate into silver clusters (Figure 3a−c). The combination of the thermodiffusion and of the central photodissociation leads to the localization and the stabilization of the clusters in the border of the irradiated zone, forming thus the ring shape.

Second, the fluorescence intensity depends linearly on the irradiance and logarithmically on the deposited number of pulses. This last behavior is similar to silver photographic film processes in which the contrast depends logarithmically with the exposure and is linked to the number of photoproduced species.[22] The silver clusters can emit fluorescence intensities (Figure 3a) much higher (10 times) than common fluorescent molecule solution (Rhodamine 6G at 10^{-4} mol·L^{-1}), without exhibiting a photobleaching effect. This strong fluorescence property has also been observed by Dickson and co-workers.[23,24] Therefore, by adjusting properly the dose, one can control the fluorescence intensity of the photoinduced species exactly like in silver photographic films.

Third, the emission spectra are dependent on both the irradiance and the number of pulses (Figure 3d,e). At a low dose, one major contribution at 1.94 eV (640 nm) and a shoulder at around 2.5 eV (500 nm) are observed; they are labeled as bands I and III, respectively (Figure 3d). When increasing the dose, a new band at 2.11 eV (590 nm), labeled as band II, becomes preponderant, whereas band I decreases and band III slightly increases (Figure 3e). Bands II and III appear at high doses and are, therefore, linked to the creation of a high concentration of electron−hole traps. When increasing the irradiance from 7 to 10 TW·cm^{-2} while keeping the number of pulses constant at 10^7, the intensity of band I falls dramatically compared with the intensity of bands II and III. This behavior describes likely a consumption of the silver clusters responsible for band I to create larger clusters related to band II and in a less important way to band III. By adjusting appropriately the dose, the emission can be tuned from red (Figure 3d) to yellow colors (Figure 3e). Using a sodium−alumino−phosphate glass with 0.07 mol % of silver similar to the radio-photoluminescent

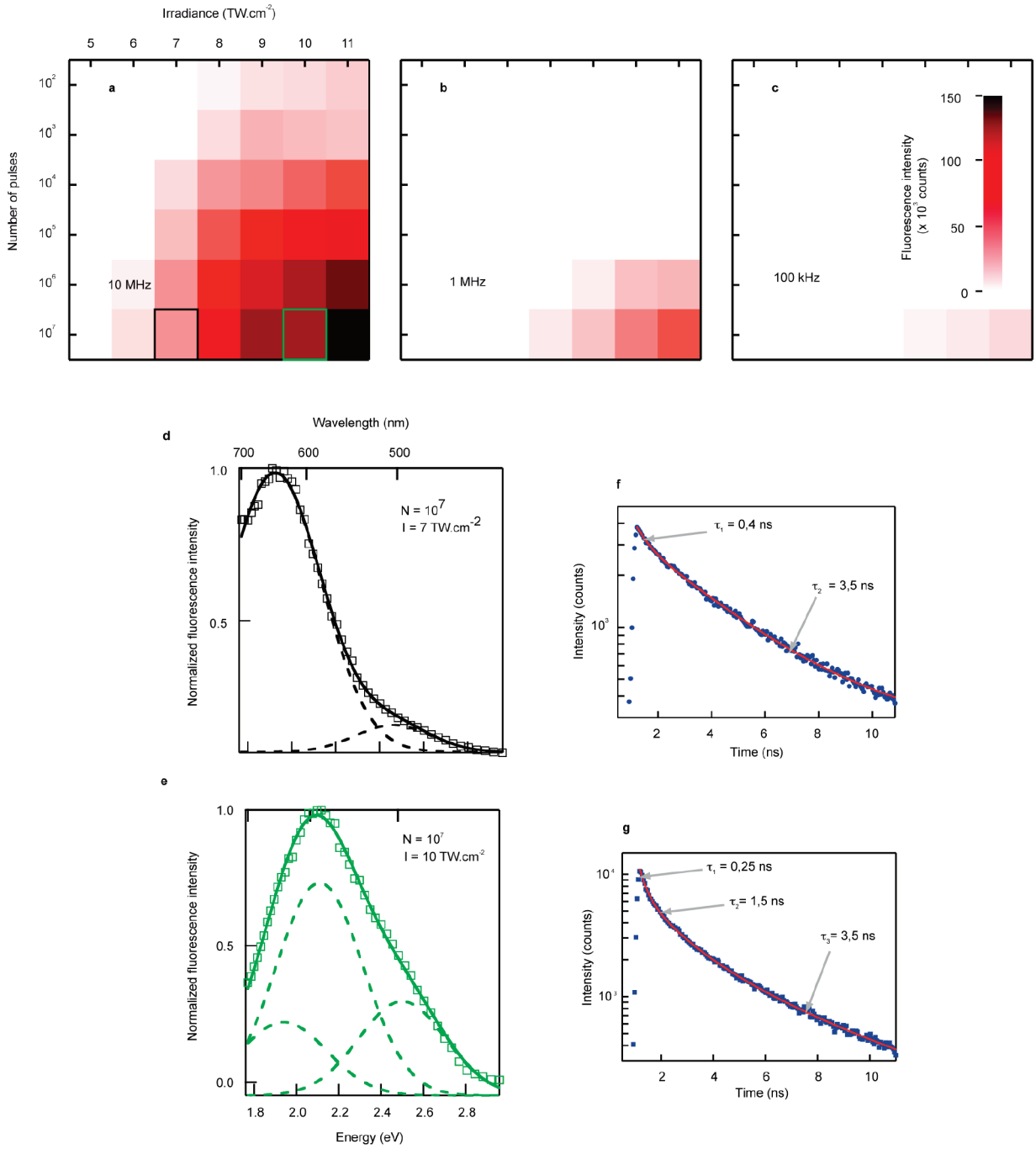

Figure 3. Fluorescence control. Maps showing the fluorescence intensity from several dots written with different irradiances and number of pulses with 10 MHz (a), 1 MHz (b), and 100 kHz (c) repetition rates. The excitation wavelength is 405 nm. Normalized fluorescence spectra of the framed dots in black (d) and green (e), corresponding to irradiances of 7 and 10 TW·cm^{-2} and 10^7 pulses at 10 MHz. The spectra were fitted using a sum of Gaussian functions in which the fwhm was fixed at 0.29 eV. Three contributions located at 1.94, 2.1, and 2.5 eV, called, respectively, bands I, II, and III, have been used for the fitting. Panels (f) and (g) are the impulse response of the emission spectra (d) and (e), respectively.

(RPL) glasses, only band I at around 640 nm can be observed. In such a glass, the photoinduced structures are unstable and bleach under intense blue radiation (dose of 57 MJ·cm^{-3} at 405 nm).

The spectra recorded in the FPL glass for low laser irradiances (Figure 3d) exhibit comparable contributions to those observed for samples irradiated with ionizing radiations, such as γ-rays, or with an electron beam for low irradiation dosages (see the Supporting Information). According to the recorded emission spectra, even if the mechanism of formation of the luminescent species is different, comparisons can be drawn based on the luminescence properties. In the case of RPL glasses (γ-dosimeter) exposed to γ-radiation, the reported emission corresponds to an emission band observed at 1.94 eV (640 nm) and has been attributed by Dmitryuk et al. to Ag_3^{2+} species using combined luminescence measurements and electron spin resonance (ESR).[9] Because the issue was to detect low γ-irradiation dosage, efforts have been concentrated on low silver ion content sodium phosphate glasses and also on the emission band recorded at around 630 nm.

Band I observed in the FPL glass could be related to the band at 630 nm reported in RPL glasses. Recently, it was demonstrated that high γ-radiation dosages or electron irradiation lead to the formation of an emission band at around 630 nm, but

also around 500 nm.[25] For the FPL glass, the fluorescence features (bands I, II, and III) observed following femtosecond laser irradiation correspond to a decrease of the intensity of the intrinsic emission at 380 nm related to the consumption of isolated silver ions and can be described as a so-called first-order kinetic reaction. On the basis of these results, one can attribute the bands at 500 nm (band I) and 590 nm (band II) to Ag_m^{x+} clusters with a high m/x ratio and the band at 640 nm (band III) to Ag_m^{x+} clusters with a low m/x ratio. When irradiated with a high repetition rate femtosecond laser for irradiances higher than 8 TW·cm^{-2}, the spectra present a preponderant band II.

The emission lifetimes of the silver clusters have been measured. Figure 3f,g corresponds to the emission spectra of Figure 3d,e, respectively. The emission lifetime associated with band I has been measured to be at the microsecond range in RPL glasses.[26] In the present work, the lifetimes recorded are on the order of a few nanoseconds. Such fast decay components are predominant and indicate that new species are formed. The impulse response of the silver clusters presents two or three decay times characteristic of the created species. Although it is difficult to correlate the time decay to a given silver nanocluster, the "short" decay time (1.5 ns) evolves with the irradiation conditions and is strongly related to the growth of band II.

3.5. Silver Cluster Stability. Finally, the stability of the photoinduced species is investigated. The photoinduced silver clusters in the FPL glass are stable in time and temperature (up to 350 °C)[16] and exhibit no photobleaching, unlike what is observed in low silver content sodium−alumino−phosphate glasses similar to regular RPL glasses. At the stage of our investigation, it is not clear if the main issues concern the amount of silver ions or the absence of sodium ions. Indeed, as previously reported for RPL glasses, the concentration of sodium ions has an important impact on the diffusion of silver species and stabilization of luminescence centers.[9] It is also of importance to take into account that, with a high repetition rate femtosecond laser, the temperature during the irradiation is above 350 °C, inducing, therefore, relaxation of the unstable species.

4. Conclusion

In conclusion, we have demonstrated the fabrication of fluorescent nanostructures in an FPL silver-containing glass by femtosecond laser direct writing. These shapable structures are composed of stabilized silver clusters. Their formation and their properties are clearly related to threshold effects. Indeed, their size can be controlled by adjusting the irradiance while their wall thickness remains constant at around 80 nm, well below the diffraction limit. Concerning their remarkable luminescent properties (high intensity, visible spectrum, short lifetime, no photobleaching), they are governed by the dose and can, therefore, be controlled as well. The silver concentration and temperature effects seem to be the relevant issues for stabilization of the luminescent centers. Within this context, the design of 3D fluorescent nanostructures can easily be achieved and one can find numerous applications in optical data storage and nanophotonics.

Acknowledgment. The authors acknowledge Sonia Gomez and the CREMEM platform (ICMCB-CNRS-University of Bordeaux) for the HRSEM images and Philippe Legros, Christel Poujol, and the Bordeaux Imaging Center (Neurosciences Institute of the University of Bordeaux) for the confocal fluorescence microscopy. This work has been supported by the Aquitaine Region, the GIS AMA, the NSF, and a FACE grant from the French Embassy in the U.S.

Supporting Information Available: Information concerning nanoscale analysis, excitation spectra, and comparison of the fluorescence properties from different irradiation sources. This material is available free of charge via the Internet at http://pubs.acs.org.

References and Notes

(1) Leitner, A.; Lippitsch, M. E.; Draxler, S.; Riegler, M.; Aussenegg, F. R. *Appl. Phys. B: Lasers Opt.* **1985**, *36*, 105.
(2) Fedrigo, S.; Harbich, W.; Buttet, J. *J. Chem. Phys.* **1993**, *99*, 5712.
(3) Marchetti, A. P.; Muenter, A. A.; Baetzold, R. C.; McCleary, R. T. *J. Phys. Chem. B* **1998**, *102*, 5287.
(4) Xiao, L.; He, Y.; Yeung, E. S. *J. Phys. Chem. C* **2009**, *113*, 5991.
(5) Xu, H.; Suslick, K. S. *Adv. Mater.* **2010**, *22*, 1.
(6) Zhang, J.; Xu, S.; Kumacheva, E. *Adv. Mater.* **2005**, *17*, 2336.
(7) Becker, K. *At. Energy Rev.* **1967**, *5*, 43.
(8) Schneckenburger, H.; Regulla, D. F.; Unsöld, E. *Appl. Phys. A: Mater. Sci. Process.* **1981**, *26*, 23.
(9) Dmitryuk, A. V.; Paramzina, S. E.; Perminov, A. S.; Solov'eva, N. D.; Timofeev, N. T. *J. Non-Cryst. Solids* **1996**, *202*, 173.
(10) Treguer, M.; Rocco, F.; Lelong, G.; Le Nestour, A.; Cardinal, T.; Maali, A.; Lounis, B. *Solid State Sci.* **2005**, *7*, 812.
(11) Stookey, S. D. *Ind. Eng. Chem.* **1949**, *41*, 856.
(12) Gattass, R. R.; Mazur, E. *Nat. Photonics* **2008**, *2*, 219.
(13) Miura, K.; Qiu, J.; Inouye, H.; Mitsuyu, T.; Hirao, K. *Appl. Phys. Lett.* **1997**, *71*, 3329.
(14) Zoubir, A.; Richardson, M.; Canioni, L.; Brocas, A.; Sarger, L. *J. Opt. Soc. Am. B* **2005**, *22*, 2138.
(15) Glezer, E. N.; Milosavljevic, M.; Huang, L.; Finlay, R. J.; Her, T.-H.; Callan, J. P.; Mazur, E. *Opt. Lett.* **1996**, *21*, 2023.
(16) Canioni, L.; Bellec, M.; Royon, A.; Bousquet, B.; Cardinal, T. *Opt. Lett.* **2008**, *33*, 36.
(17) Sun, H. B.; Tanaka, T.; Takada, K.; Kawata, S. *Nature* **2001**, *412*, 697.
(18) Johnson, S. G.; Joannopoulos, J. D. *Appl. Phys. Lett.* **2000**, *77*, 3490.
(19) Rill, M. S.; Plet, C.; Thiel, M.; Staude, I.; von Freymann, G.; Linden, S.; Wegener, M. *Nat. Mater.* **2008**, *7*, 543.
(20) Belharouak, I.; Parent, C.; Tanguy, B.; Le Flem, G.; Couzi, M. *J. Non-Cryst. Solids* **1999**, *244*, 238.
(21) Bellec, M.; Royon, A.; Bousquet, B.; Bourhis, K.; Treguer, M.; Cardinal, T.; Richardson, M.; Canioni, L. *Opt. Express* **2009**, *17*, 10304.
(22) Biedermann, K. *Appl. Opt.* **1971**, *10*, 584.
(23) Peyser, L. A.; Vinson, A. E.; Bartko, A. P.; Dickson, R. M. *Science* **2001**, *291*, 103.
(24) Vosch, T.; Antoku, Y.; Hsiang, J. C.; Richards, C. I.; Gonzalez, J. I.; Dickson, R. M. *Proc. Natl. Acad. Sci. U.S.A.* **2007**, *104*, 12616.
(25) Maurel, C.; Cardinal, T.; Bellec, M.; Canioni, L.; Bousquet, B.; Treguer, M.; Videau, J. J.; Choi, J.; Richardson, M. *J. Lumin.* **2009**, *129*, 1514.
(26) Schulman, J. H.; Ginther, R. J.; Klick, C. C.; Alger, R. S.; Levy, R. A. *J. Appl. Phys.* **1951**, *22*, 1479.

JP104049E